Influence of the boundary conditions on heat and mass transfer in spacer-filled channels

IOP Conf. Series: Journal of Physics: Conf. Series **923** (2017) 012053 doi:10.1088/1742-6596/923/1/012053

Influence of the boundary conditions on heat and mass transfer in spacer-filled channels

M Ciofalo, M F La Cerva, M Di Liberto and A Tamburini

Dipartimento dell'Innovazione Industriale e Digitale, Università di Palermo, Italy
E-mail michele.ciofalo@unipa.it

Abstract. The purpose of this study is to discuss some problems which arise in heat or mass transfer in complex channels, with special reference to the spacer-filled channels adopted in membrane processes. Among the issues addressed are the consistent definition of local and mean heat or mass transfer coefficients; the influence of the wall boundary conditions; the influence of one-side versus two-side heat/mass transfer. Most of the results discussed were obtained by finite volume CFD simulations concerning heat transfer in Membrane Distillation or mass transfer in Electrodialysis and Reverse Electrodialysis, but many of the conclusions apply also to different processes involving geometrically complex channels.

1. Heat and mass transfer in spacer-filled channels

Membrane processes offer examples of heat or mass transfer in plane channels bearing mixing promoters of more or less tortuous geometry, aimed at reducing temperature or concentration polarization phenomena thus improving the process performance [1, 2]. Promoters usually consist of polymeric filaments and play also the role of spacers, keeping a fixed distance between the opposite channel walls. For example, the top row in Figure 1 shows real spacers made of overlapped (a) or woven (b) filaments. The bottom row shows corresponding unit cells (computational domains).

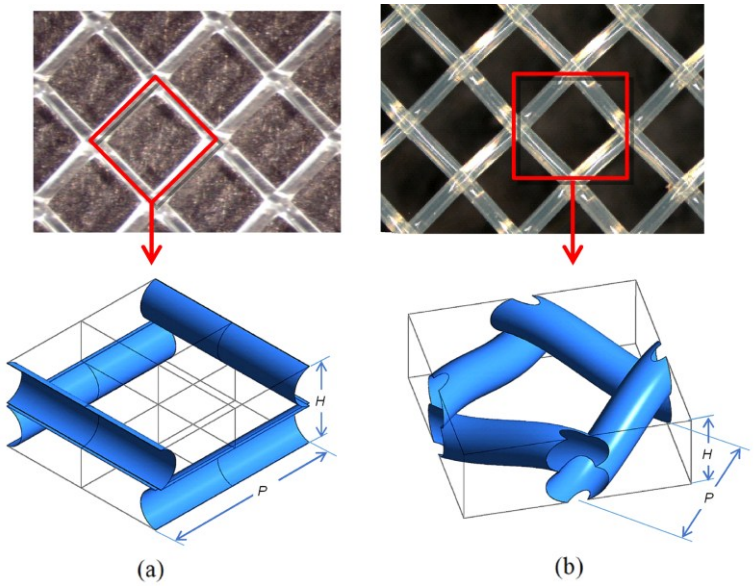

Figure 1. Lattice (top row) and unit cells (bottom row) of spacer-filled channels. (a) overlapped; (b) woven.

CFD simulations of spacer-filled channels for membrane processes started to appear in the literature since the year 2001 and have been presented at an increasing rate since then. Hitsov *et al.* [3], Fimbres-Wehis and Wiley [4], Karabelas *et al.* [5] and La Cerva *et al.* [6] have presented reviews addressing a number of issues in the modeling of such channels.

The present paper aims to complement the above reviews, by discussing a number of aspects not sufficiently clarified so far. The main issues addressed here are:

- the consistent definition of local and mean heat or mass transfer coefficients;
- the influence of the wall boundary conditions;
- the influence of one-side versus two-side heat/mass transfer.

Most of the results that follow make reference to the spacer geometry Diamond_90 in Figure 1(a), consisting of identical overlapping cylindrical filaments with an intrinsic angle α=90° and different flow attack angles γ and Reynolds numbers Re.

The problem is described by the continuity, Navier-Stokes and scalar transport equations for a constant-property fluid. For simplicity, in the following the transported scalar will be assumed to be the specific enthalpy c_pT; obvious changes apply in the case of mass transport.

In order to simulate fully developed flow and thermal fields by simply applying periodicity conditions at the opposite faces, "true" pressure p^* and temperature T^* are replaced by their periodic components p, T such that

$$p^* = p + p_s s \tag{1}$$

$$T^* = T + T_s s \tag{2}$$

in which s is the distance along the streamwise (main flow) direction while p_s and T_s are the large-scale gradients of pressure and temperature, respectively, in the same direction. Note that p_s is always negative while T_s is positive for a heated fluid and negative for a cooled fluid.

In the simulations, the pressure gradient p_s is imposed while the flow rate and thus the bulk flow Reynolds number Re follow as results of the simulation.

As regards the large-scale temperature gradient, a heat balance yields $T_s=q/(\rho c_p UV)$ in which U is the mean "void channel" velocity in the direction s, V is the volume of the unit cell and q is the thermal power entering the fluid from the walls of the same cell. Both q and U are evaluated as parts of the solution during the course of the simulation.

Substituting eqs. (1)-(2) for p^* and T^* in the standard steady-state momentum and energy equations, after some manipulation one obtains the following governing equations (written in Cartesian tensor notation):

$$\frac{\partial \rho u_j}{\partial x_j} = 0 \tag{3}$$

$$\frac{\partial \rho u_i u_j}{\partial x_j} = -\frac{\partial p}{\partial x_i} + \frac{\partial}{\partial x_j}\mu\frac{\partial u_i}{\partial x_j} - p_s\frac{\partial x_i}{\partial s} \tag{4}$$

$$\frac{\partial \rho c_p u_j T}{\partial x_j} = \frac{\partial}{\partial x_j}\lambda\frac{\partial T}{\partial x_j} - \frac{q}{V}\frac{u_s}{U} \tag{5}$$

in which u_s is the component of the local velocity along the direction s.

Translational periodic boundary conditions were now adopted for all variables at the opposite faces of the computational domain. No slip conditions (u_i=0) were imposed at the top and bottom walls and on the filaments' surface. As regards the thermal boundary conditions, the filaments were assumed to be adiabatic (q"=0), while at either one or both the walls different thermal boundary conditions were imposed, as will be discussed below.

All simulations were conducted by the ANSYS-CFX® code. The code uses a finite volume approach and a co-located (non-staggered) grid layout, such that the control volumes are identical for all transport equations. A coupled solver is adopted, in which the hydrodynamic equations for the three velocity components and pressure are treated as a single large system. A Multi-grid (MG) accelerated Incomplete Lower Upper (ILU) factorization technique is adopted for solving the discrete system of linearized equations.

In the present simulations, the "high resolution" (higher order upwind) interpolation scheme was used for the advection terms. Further numerical methods and computational details have been discussed elsewhere [7, 8].

2 Definition of local or averaged heat / mass transfer coefficients

2.1 Local coefficients

Making reference, for the purpose of clarity, to heat transfer, the most common definition of the local heat transfer coefficient is:

$$h = \frac{q''_w}{T_b - T_w} \tag{6}$$

In Eq. (6) q''_w is the local wall heat flux (assumed to be positive for a cooled fluid), T_w is the local wall temperature and T_b is the bulk temperature, usually defined as:

$$T_b = \int_A \rho c_p T u_s \mathrm{d}A \quad / \quad \int_A \rho c_p u_s \mathrm{d}A \tag{7}$$

A being the cross sectional area of the channel. Often ρ and c_p can be treated as constant properties. Note that T_b remains a function of s. When the computational domain is a single repetitive unit of a large lattice (unit cell approach) it may be preferable to define the bulk temperature by replacing the area integrals in Eq. (7) with volume integrals taken over a whole unit cell. Yet another alternative is to replace the bulk temperature in the definition (6) of h with a different reference value, e.g. the fluid's temperature at the channel midplane [9] or the fluid's inlet temperature [10].

In the case of mass transfer, temperature is replaced by concentration and h is replaced by a mass transfer coefficient k (in m s^{-1}).

The problem with the above definition of h or k is that, in complex geometries involving flow recirculation, the iso-surface $T=T_b$ (or $C=C_b$) may intersect the channel walls; in this case, h (k) diverges on the line $T_b=T_w$ ($C_b=C_w$) and becomes negative inside this line. An example is reported in Figure 2, obtained by post-processing the results of a three-dimensional CFD simulation. It shows the iso-surface $T=T_b$ (bulk temperature) for an overlapped spacer with $P/H=4$, $\gamma=0°$, Re≈42 and two-side heat transfer with uniform imposed wall heat flux. Even in the absence of singularities, the simple fact that the iso-surface $T=T_b$ (or $C=C_b$) approaches the wall closely may give rise to abnormal and unphysically large values of h or k. This kind of distribution is rather common, especially for imposed flux (2nd type) or mixed (3rd type) boundary conditions, two-side heat / mass transfer, high Reynolds numbers and high Prandtl / Schmidt numbers. The only condition in which singularities cannot occur is that of imposed wall temperature or concentration (1st type, or Dirichlet).

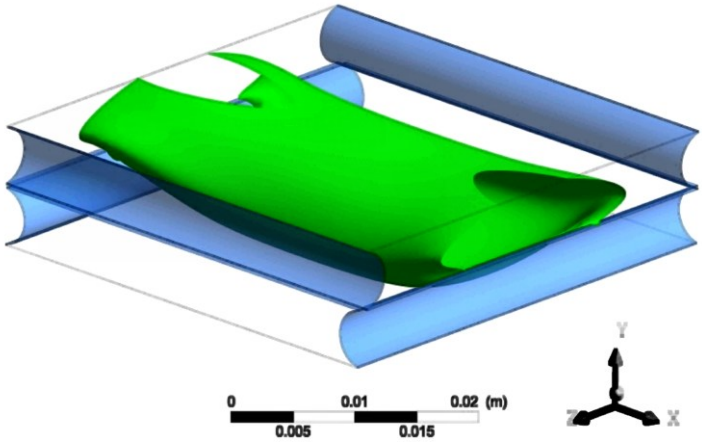

Figure 2. Iso-surface $T=T_b$ (bulk temperature) for an overlapped spacer with $P/H=4$, $\gamma=0°$, Re≈42 and two-side heat transfer with uniform imposed wall heat flux.

2.2 Average coefficients

In most papers dealing with heat or mass transfer in spacer-filled channels [9, 11, 12, 13], the average transfer coefficient is simply defined as the area average

$$h^{(1)} = \langle h \rangle = \frac{1}{S}\int_S h \, \mathrm{d}S = \frac{1}{S}\int_S \frac{q''_w}{T_b - T_w}\,\mathrm{d}S \tag{8}$$

where S may be the whole active transfer surface or a sub-region of it (e.g., one of two active channel walls). Obvious modifications apply if mass transfer is considered.

The problem with this definition is that, if the local h (or K) is singular or attains unphysical values (for the reasons discussed just above), also its average $\langle h \rangle$ (or $\langle K \rangle$) will be affected by this behavior. A preferable definition of the averages, which does not suffer from this problem, is [7, 8]

$$h^{(2)} = \frac{\langle q''_w \rangle}{T_b - \langle T_w \rangle} \tag{9}$$

in which $\langle q''_w \rangle$ and $\langle T_w \rangle$ are surface averages of q''_w or T_w over the surface of interest (e.g., one or both walls). Obvious modifications apply in the case of mass transfer. Dimensionless numbers $\mathrm{Nu}^{(1)}$, $\mathrm{Nu}^{(2)}$ or $\mathrm{Sh}^{(1)}$, $\mathrm{Sh}^{(2)}$ can be obtained from the above definitions by choosing a suitable length scale.

$\mathrm{Nu}^{(1)}$ and $\mathrm{Nu}^{(2)}$ coincide when a uniform wall temperature is imposed, while they differ when a uniform wall heat flux or a wall thermal resistance are imposed. In fact, one can write:

$$\mathrm{Nu}^{(1)} = \mathrm{constant} \times \left\langle \frac{q''_w}{\Delta T_{bw}} \right\rangle, \qquad \mathrm{Nu}^{(2)} = \mathrm{constant} \times \frac{\langle q''_w \rangle}{\langle \Delta T_{bw} \rangle} \tag{10}$$

in which $\Delta T_{bw} = T_b - T_w$. When T_w is imposed, ΔT_{bw} is a constant (say, $\Delta T_{bw}{}^0$) and one has

$$\mathrm{Nu}^{(1)} = \mathrm{Nu}^{(2)} = \mathrm{constant} \times \frac{\langle q''_w \rangle}{\Delta T^0_{bw}} \tag{11}$$

On the contrary, when a uniform heat flux is imposed, q''_w is a constant (say, $q''_w{}^0$) and one has

$$\mathrm{Nu}^{(1)} = \mathrm{constant} \times q''^0_w \left\langle \frac{1}{\Delta T_{bw}} \right\rangle \neq \mathrm{Nu}^{(2)} = \mathrm{constant} \times q''^0_w \frac{1}{\langle \Delta T_{bw} \rangle} \tag{12}$$

since the average of the reciprocal is *not* the reciprocal of the average.

The difference between the two definitions is illustrated in Figure 3, which reports average Nusselt and Sherwood numbers, computed by using definitions (8) and (9) for the average heat (mass) transfer coefficients and $2H$ as the length scale. They are reported as functions of the Reynolds number for an overlapped spacer with P/H=4, γ=45° and two-side heat / mass transfer. The values 4 and 600 were assumed for the Prandtl and Schmidt numbers Pr and Sc, respectively, and 3rd type boundary conditions were imposed at the walls. It can be observed that $Nu^{(2)}$ and $Sh^{(2)}$ are always lower than $Nu^{(1)}$ and $Sh^{(1)}$, and that the difference increases with Re. Note also that the difference between $Sh^{(1)}$ and $Sh^{(2)}$ (Sc=600) is larger than that between $Nu^{(1)}$ and $Nu^{(2)}$ (Pr=4).

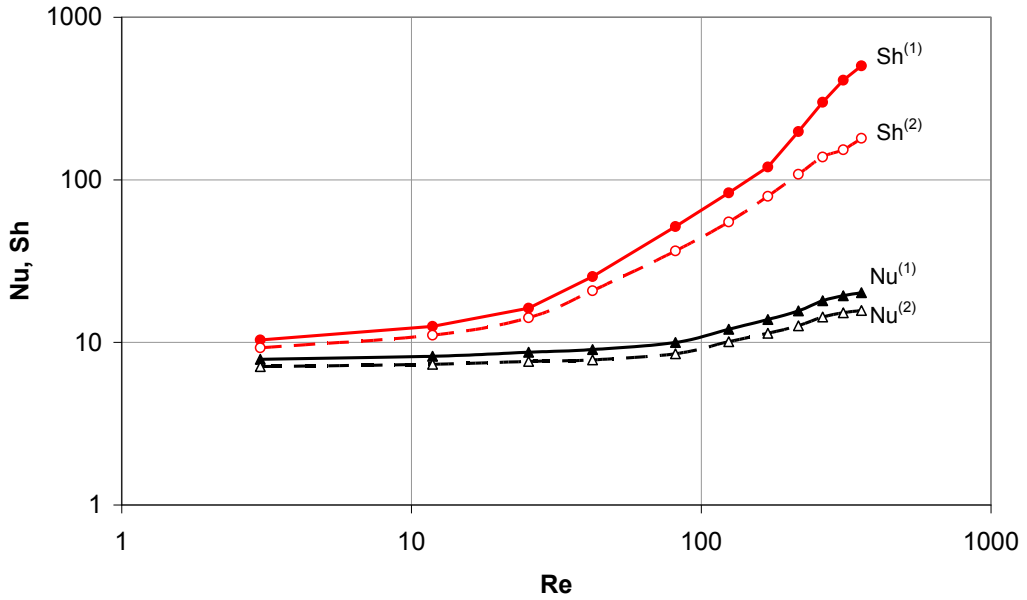

Figure 3. Average Nusselt and Sherwood numbers, computed by definitions (1) and (2), as functions of the Reynolds number for an overlapped spacer with l/H=4, flow attack angle γ=45°, two-side heat / mass transfer and 3rd type boundary conditions (Prandtl number Pr=4, Schmidt number Sc=600).

3 Influence of the boundary conditions at the walls

The different boundary conditions that can be imposed at a wall for a scalar transport equation are schematically illustrated in Figure 4. For the purpose of clarity, reference is made to temperature and heat transfer; obvious modifications apply if concentration and mass transfer are considered instead.

The different BC's can be regarded as particular cases of the most general 3rd type condition :

$$T_w - T_{ext} = r_{ext}\, q''_w \tag{13}$$

in which T_w is the wall temperature; T_{ext} is the temperature of some external medium; r_{ext} is the interposed thermal resistance per unit wall area, inclusive of the conductive resistance of the membrane and (if appropriate) of the convective resistance on the opposite fluid flow; and q''_w is the wall heat flux. This is made clear by writing

$$q''_w = \frac{T_b - T_{ext}}{r_{ext} + 1/h} \tag{14}$$

in which h is the convective heat transfer coefficient. Case (a) is obtained for $r_{ext} \ll 1/h$ and approaches uniform wall temperature (1st type, or Dirichlet) conditions; case (b) applies to a generic condition; case (c) is obtained for $r_{ext} \gg 1/h$, and approaches uniform heat flux (2nd type, or Neumann) conditions.

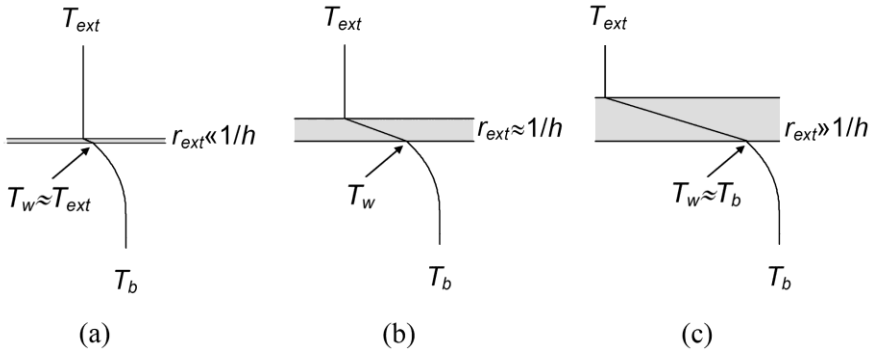

Figure 4. Thermal boundary conditions at a wall obtained as particular cases of the general 3rd type condition for different values of the ratio between the wall thermal resistance r_{ext} and the convective heat transfer resistance $1/h$. (a) Case $r_{ext}«1/h$, approaching uniform wall temperature (1st type, or Dirichlet) conditions; (b) generic case ($r_{ext}≈1/h$); (c) case $r_{ext}»1/h$, approaching uniform heat flux (2nd type, or Neumann) conditions.

The thermal resistance r_{ext} can be made dimensionless as $R=r_{ext}\lambda_f/\delta$, in which λ_f is the thermal conductivity of the fluid and δ is the channel's half-height (other choices of the reference length are, of course, possible). Accurate solutions for the Nusselt number under any prescribed value of R can be obtained for the case of a (void, or spacerless) plane channel, as described in detail in the Appendix. Figure A.1 therein reports the Nusselt number (based on the hydraulic diameter $2H$ of the void channel) as a function of R both for two-side and one-side heat transfer. The limiting conditions $R\to 0$ (uniform wall temperature) and $R\to\infty$ (uniform wall heat flux) are also reported. It can be observed that thermal boundary conditions affect the Nusselt number to a significant extent, and that Nu is always increasing with R both for one-side and for two-side transfer.

In a real spacer-filled channel for membrane processes, the actual boundary conditions will be, in general, of some intermediate type, with an external resistance r_{ext} and an external temperature T_{ext} that will depend on the specific process. For example, in Direct Contact Membrane Distillation r_{ext} may represent the thermal resistance of the membrane itself in series with the condensation thermal resistance on the permeate side, and T_{ext} will be the condensing temperature. In numerical simulations, most authors imposed at the walls either a uniform temperature / concentration [11] or a uniform heat / mass flux [14, 15, 16]. Tamburini *et al.* [7] simulated their own experiments on Membrane Distillation, conducted under one-sided heat transfer (see also following Section), by imposing the mixed (3rd type) boundary condition of Eq. (7) with r_{ext}=0.00625 m^{2}K/W (corresponding to R=0.75 for the geometry investigated) at one of the walls (active, top wall), the opposite wall being adiabatic. Only Shakaib *et al.* [10] explicitly simulated both the hot and the cold fluid, thermally coupled through a membrane of prescribed thickness and thermal conductivity.

In the present work, in order to study how the Nusselt number in a spacer-filled channel is affected by the thermal resistance, simulations were repeated for different geometric configurations and Reynolds numbers letting R vary between 0 and 100. Figure 5 shows the behavior of the averages $Nu^{(1)}$ and $Nu^{(2)}$ as functions of R for one-side heat transfer, γ=45° and P/H=4, Re≈42 (graph a) or P/H=2, Re≈126 (graph b).

The more reliable of the two averages, i.e., $Nu^{(2)}$, decreases monotonically with R in both cases; the highest values of $Nu^{(2)}$ are attained for R=0 (isothermal wall conditions) and the lowest for $R\to\infty$. Note that this behavior is opposite to that reported in the Appendix for the case of a spacerless channel, where Nu *increases* monotonically with R and thus is larger for an imposed uniform wall heat flux than for an imposed uniform wall temperature. This is not surprising since spacer-filled channels exhibit a strong and complex non-uniformity of heat transfer rates over the active wall surface of each unit cell, whereas a spacerless plane channel exhibits only a large-scale longitudinal variation of wall temperature and/or heat flux.

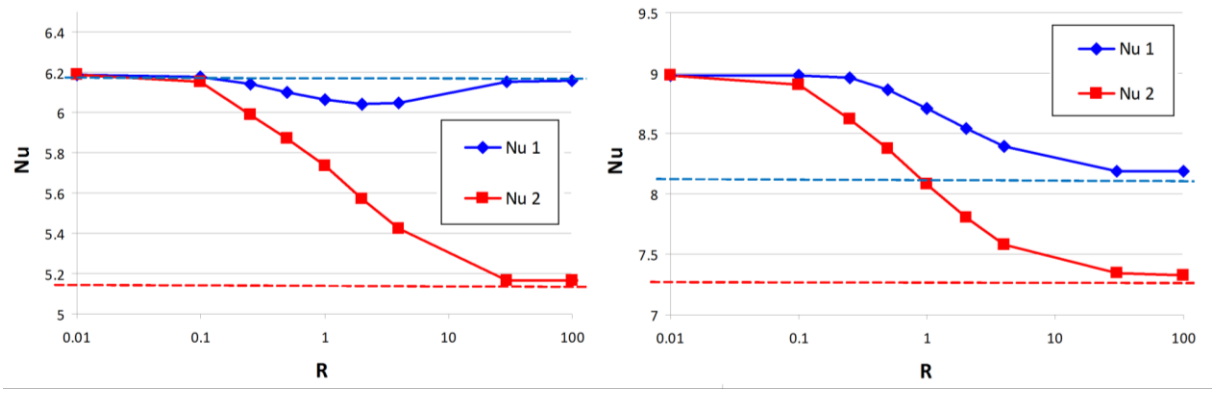

Figure 5. Dependence of the average Nusselt numbers $Nu^{(1)}$ and $Nu^{(2)}$ on the dimensionless wall resistance R for one-side heat transfer in a spacer-filled channel (overlapped, γ=45°). (a) P/H=4, Re≈42; (b) P/H=2, Re≈126. Broken lines are the theoretical values of Nu in a plane (spacerless) channel for $R\to 0$ (red) and $R\to\infty$ (blue).

For P/H=4, γ=0°, Re≈42 and one-side heat transfer, Figure 6 shows the influence of thermal boundary conditions on the local distributions of wall temperature (top row), local Nusselt number (middle row) and heat flux (bottom row). The left column is for R=0 (uniform wall temperature); the central column is for R=0.75 (mixed, or 3rd type boundary condition); finally, the right column is for $R\to\infty$ (uniform wall heat flux).

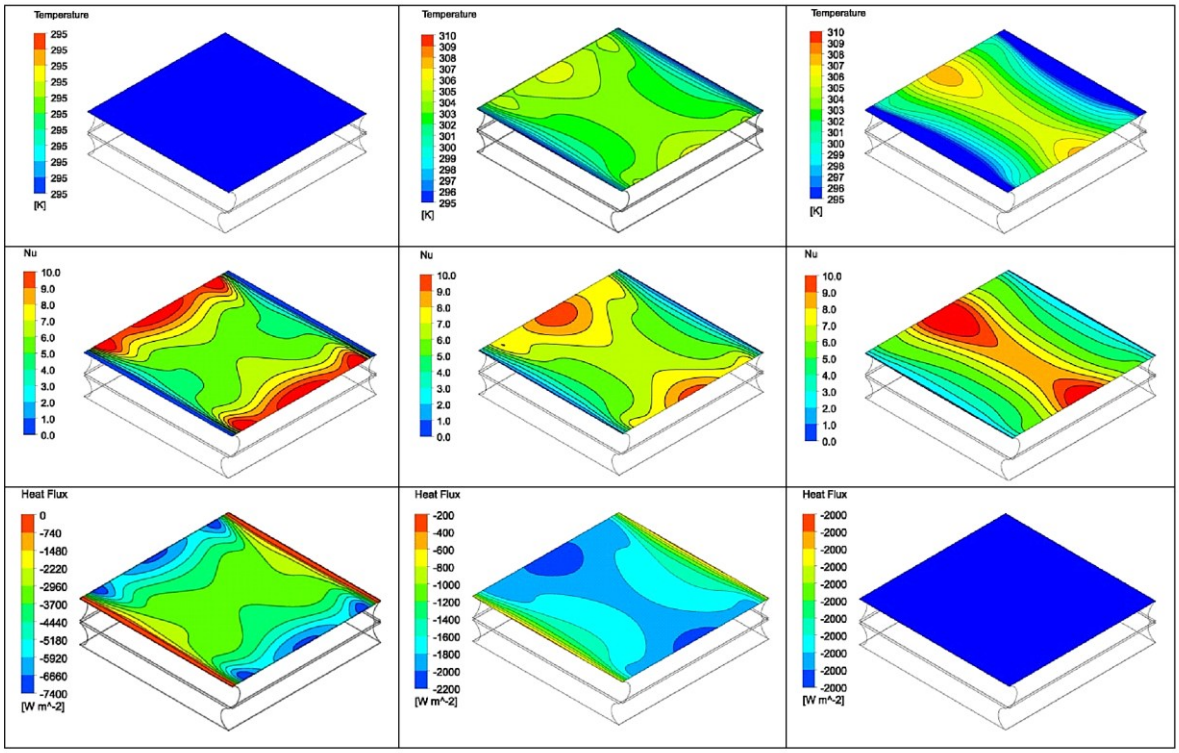

Figure 6. Computed top wall distributions for P/H=4, γ=0°, Re≈42, one-side heat transfer and different thermal boundary conditions: R=0, or uniform wall temperature (left), R=0.75, or general 3rd type boundary conditions (centre), and $R\to\infty$, or uniform wall heat flux (right). Top row: temperature; middle row: heat transfer coefficient; bottom row: heat flux.

Figure 6 shows that the choice of the thermal boundary conditions at the wall affects the local distributions of thermal quantities even more than it affects average quantities such as $Nu^{(2)}$. Therefore, in studies discussing the wall distributions of thermal quantities, and even more so in studies comparing experimental and predicted results for the same quantities, a realistic choice of the thermal boundary conditions appears to be crucial.

Needless to say, the above considerations can be adapted to *mass* transfer by a suitable change of notation, provided realistic values are adopted for the membrane resistance to mass transfer.

4 One-side against two-side heat / mass transfer

A fluid-filled channel can be subjected to different types of heat or mass transfer on the two sides, as sketched in Figure 7 for the case of heat transfer. Case (a) is heat transfer from one-side with the opposite side wall adiabatic. Case (b) is two-side asymmetric heat transfer with heat inflow from one side and outflow from the opposite side. Finally, case (c) is two-side symmetric heat transfer with heat inflow or outflow from both sides. Indicative bulk and wall temperatures are also shown in the figures; of course, in all cases the sign of T_w-T_b is arbitrary.

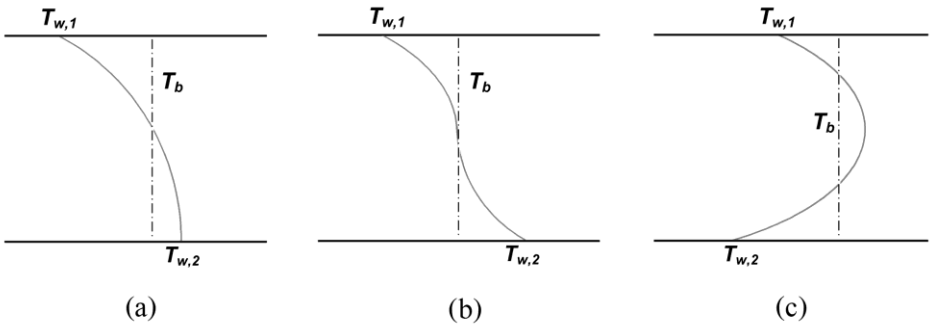

Figure 7. Possible heat transfer arrangements in membrane processes. (a) one-side heat transfer with one adiabatic wall; (b) two-side asymmetric heat transfer with heat inflow from one side and outflow from the opposite side; (c) two-side symmetric heat transfer with heat inflow or outflow from both sides. Representative temperature profiles and bulk and wall values of T are shown.

In the case of Membrane Distillation (MD), case (a) (one-side heat transfer) is usually realized in laboratory-scale experimental rigs [7, 17, 18] or small-scale, plate-and-frame, MD equipment [19, 20] because it is simpler to build and allows an easier experimental characterization of temperatures and heat fluxes.

Case (b) (heat inflow from one side of the channel, outflow from the opposite side) is found, for example, in the Memsys™ modules adopted in Vacuum Multi Effect Membrane Distillation (V-MEMD) [21], in which the generic stage is powered by the condensation heat from a previous stage, thus saving the thermal energy that otherwise should be provided from the outside. One side of each channel is provided with a microporous membrane allowing the passage of vapor, while the other side is a thin polypropylene sheet, on the outside of which the vapor from the previous stage condenses.

Most commercial MD plant usually exhibit outwards (though not necessarily symmetric) heat and mass transfer from both sides of the feed channels, case (c). An example are the spiral wound modules developed at the Fraunhofer Institute [22], in which the hot (feed) channel is placed between two membranes followed by two condensate channels, two conductive walls and two cooling channels, and the whole arrangement is then spirally wound to achieve compactness and reduce heat losses. The feed channel is usually provided with a spacer (not shown).

Among computational studies of membrane processes, both the one-side configuration (a) [7, 10, 14, 23, 24] and the two-side, symmetric configuration (c) [11, 9, 13] have been considered.

For the case of a spacerless plane channel subjected to hydrodynamically and thermally fully developed flow, the difference in the Nusselt numbers for one-side and two-side heat transfer is illustrated in Figure A.1. It can be observed that two-side heat transfer yields Nusselt numbers higher by a factor ~1.5 with respect to one-side transfer for any given dimensionless thermal resistance R. Therefore, switching from one-side to two-side heat transfer causes an increase of the total heat exchanged by about three times.

The physical interpretation of the increase in the Nusselt number on a given wall (say, the top wall) caused by the occurrence of symmetric heat transfer also on the *opposite* wall (say, the bottom wall) rests on the observation that switching from one-side to two-side heat transfer moves the adiabatic condition $\partial T/\partial y=0$ at the bottom wall to a formally identical symmetry condition $\partial T/\partial y=0$ at the midplane, thus halving the actual distance between bulk fluid and wall. Since velocity profiles are not affected by thermal boundary conditions, the increase in Nu is not twofold but ~1.5 times.

For spacer-filled channels, the behavior of the Nusselt number is more complex but follows the same general trend. For example, Figure 8 compares $Nu^{(2)}$ on both walls in two-side heat transfer with $Nu^{(2)}$ on the single active (top) wall in one-side heat transfer for an overlapped spacer having $P/H=2$ and $\gamma=0°$ (a) or 45° (b). Note that the second definition of the average Nusselt number was used in order to obtain more regular and meaningful results. Note also that for $\gamma= 45°$, graph (b), the values of $Nu^{(2)}$ on the two walls are identical for symmetry reasons and, of course, coincide also with their average. It can be observed that, for $\gamma=0°$ (main flow aligned with the spacer filaments adjacent to the top wall), the Nusselt number in the case of heat transfer from the top wall only exhibits a completely different behavior than either the top- or the bottom-wall Nu in two-side heat transfer; in particular, it exhibits a large *plateau* which shrinks considerably in two-side transfer.

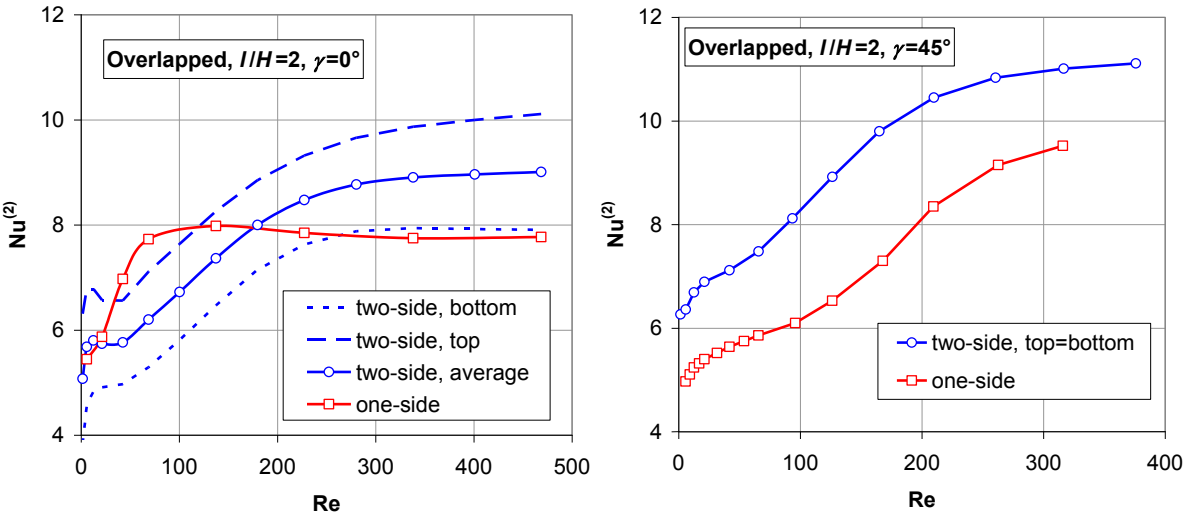

(a) (b)

Figure 8. Comparison of one- and two-side heat transfer in an overlapped spacer filled channel for $P/H=2$. The values of $Nu^{(2)}$ on the top and bottom walls and of their average in two-side heat transfer are reported as functions of the Reynolds number along with the values of $Nu^{(2)}$ on the only active wall (top wall) in one-side heat transfer. (a) $\gamma=0°$; (b) $\gamma= 45°$. Note that in this latter case one has $Nu^{(2)}_{top} = Nu^{(2)}_{bottom}$.

Once averaged between top and bottom walls, the two-side Nusselt number is lower than the single $Nu^{(2)}$ obtained in one-side transfer for Re<~180, but becomes up to 15% higher for larger values of the Reynolds number. For the flow attack angle of 45°, the trends of the two curves are similar but the two-side Nusselt number is 1.15~1.35 times higher than the one-side Nusselt number at all Re, so that the overall thermal power exchanged for any bulk to wall temperature difference is from 2.3 to 2.7 times larger (of course, the heat transferred *per unit membrane area* is only 1.15~1.35 times larger).

From these results it can be concluded that:

- in Membrane Distillation, two-side heat and mass transfer should be preferred as it generally provides larger heat transfer rates per unit membrane surface area at the Reynolds numbers (>200) expected in practical applications;
- experimental and computational results obtained for one-side transfer cannot be extended to two-side transfer, because not only the absolute values of the average Nusselt number, but also its trend with Re and other parameters, may differ significantly, and the relative performance ranking of the various configurations examined may be altered.

5 Conclusions

The main objective of the present paper was to clarify a number of issues arising in the study of fluid flow and heat/mass transfer in membrane processes involving flat, spacer-filled, channels (either plane or spirally wound). Other designs, including dead-end arrangements and tubular or hollow-fiber membranes, raise different problems which were not discussed here. The conclusions reached were based on many years' experience with Membrane Distillation and Reverse Electrodialysis, but many of them can be extended to other membrane processes as well. The results of the study can be summarized as follows:

- In regard to the definition of *local* heat or mass transfer coefficients, the definition based on the local heat / mass flux and on the difference between the local temperature or concentration at the wall and the corresponding bulk values, i.e. $h=q''_w/(T_b-T_w)$ or $k=j_w/(C_b-C_w)$, remains the most commonly adopted, but we have shown that these quantities may become singular or negative at some points of the wall in complex geometries. For this and other reasons, the definition of the average coefficients as surface averages $h^{(1)}=\langle h\rangle$, $k^{(1)}=\langle k\rangle$ (definition 1) should be avoided, and the alternative averages $h^{(2)}=\langle q''_w\rangle/(T_b-\langle T_w\rangle)$, $k^{(2)}=\langle j_w\rangle/(C_b-\langle C_w\rangle)$ (definition 2), which do not suffer from singularities, are preferable both in computational and in experimental work.
- In regard to the choice of temperature or concentration boundary conditions at the walls representing the fluid-membrane interfaces in CFD simulations, we have shown that it may have a significant impact on the computed Nusselt or Sherwood numbers, especially in laminar flow. Therefore, experimental data ought to be compared only with CFD results based on a realistic description of the actual boundary conditions, rather than with idealized cases based on uniform temperature / concentration (Dirichlet) or uniform heat / mass flux (Neumann) conditions. For design purposes, it is preferable to use convection coefficients based on generalized (3rd type) boundary conditions with some intermediate value of the wall heat / mass transfer resistance.
- In regard to the comparison between one-side and two-side heat or mass transfer, this choice has a dramatic impact on the corresponding coefficients: these may be up to 30% higher in a two-side configuration, yielding correspondingly higher heat or mass fluxes per unit membrane area. Experimental or computational results obtained for one-side transfer should not be extended to two-side transfer, because not only the values of the average Nusselt / Sherwood numbers, but also their dependence on Re and other parameters, may differ significantly, and the relative performance ranking of different configurations may be altered.

References

[1] P. Onsekizoglu, Membrane Distillation: principle, advances, limitations and future prospects in food industry, in *Distillation-Advances from Modeling to Applications*, Zereshki S. (Ed.), InTech (2012).

[2] L. Gurreri, A. Tamburini, A. Cipollina, G. Micale, M. Ciofalo, Flow and mass transfer in spacer-filled channels for Reverse Electrodialysis: a CFD parametrical study, *J. Membr. Sci.* **497** (2016) 300–317.

[3] I. Hitsov, T. Maere, K. DeSitter, C. Dotremont, I. Nopens, Modelling approaches in Membrane Distillation: a critical review, *Sep. Purif. Technol.* **142** (2015) 48–64.

[4] G. A. Fimbres-Weihs, D. E. Wiley, Review of 3D CFD modeling of flow and mass transfer in narrow spacer-filled channels in membrane modules, *Chem. Eng. Proc.* **49** (2010) 759–781.

[5] A. J. Karabelas, M. Kostoglou, C. P. Koutsou, Modeling of spiral wound membrane desalination modules and plants: review and research priorities, *Desalination* **356** (2015) 165–186.

[6] M. La Cerva, M. Ciofalo, L. Gurreri, A. Tamburini, A. Cipollina, G. Micale, On some issues in the computational modelling of spacer-filled channels for membrane distillation, *Desalination* **411** (2017) 101-111.

[7] A. Tamburini, M. Renda, A. Cipollina, G. Micale, M. Ciofalo, Investigation of heat transfer in spacer-filled channels by experiments and direct numerical simulations, *Int. J. Heat Mass Transf.* **93** (2016) 1190-1205.

[8] M. Ciofalo, F. Ponzio, A. Tamburini, A. Cipollina, G. Micale, Unsteadiness and transition to turbulence in woven-spacer filled channels for Membrane Distillation, *Journal of Physics*, in press (paper presented at the *34th UIT Heat Transfer Conf.*, Ferrara, Italy, 2-6 July 2016).

[9] C. P. Koutsou, S. G. Yiantsios, A. J. Karabelas, A numerical and experimental study of mass transfer in spacer-filled channels: effects of spacer geometrical characteristics and Schmidt number, *J. Membr. Sci.* **326** (2009) 234–251.

[10] M. Shakaib, S. M. F. Hasani, I. Ahmed, R. M. Yunus, A CFD study on the effect of spacer orientation on temperature polarization in Membrane Distillation modules, *Desalination* **284** (2012) 332–340.

[11] F. Li, W. Meindersma, A. B. de Haan, T. Reith, Optimization of commercial net spacers in spiral wound membrane modules, *J. Membr. Sci.* **208** (2002) 289–302.

[12] C. P. Koutsou, A. J. Karabelas, A novel retentate spacer geometry for improved spiral wound membrane (SWM) module performance, *J. Membr. Sci.* **488** (2015) 129–142.

[13] A. Saeed, R. Vuthaluru, H. B. Vuthaluru, Investigations into the effects of mass transport and flow dynamics of spacer filled membrane modules using CFD, *Chem. Eng. Res. and Des.* **93** (2015) 79–99.

[14] A. Cipollina, G. Micale, L. Rizzuti, Membrane Distillation heat transfer enhancement by CFD analysis of internal module geometry, *Des. and Water Treat.* **25** (2011) 195–209.

[15] M. Qureshi, M. Shakaib, CFD study for temperature and concentration profiles in membrane channels, *Proceedings Int. Conf. Energy and Sustainability*, NED University, Karachi, Pakistan (2013).

[16] S. Al-Sharif, M. Albeirutty, A. Cipollina, G. Micale, Modelling flow and heat transfer in spacer-filled Membrane Distillation channels using open source CFD code, *Desalination* **311** (2013) 103–112.

[17] A. Ali, F. Macedonio, E. Drioli, S. Aljlil, O. A. Alharbi, Experimental and theoretical evaluation of temperature polarization phenomenon in Direct Contact Membrane Distillation, *Chem. Eng. Res. and Des.* **91** (2013) 1966-1977.

[18] M. Khayet, C. Cojocaru, A. Baroudi, Modeling and optimization of sweeping gas Membrane Distillation, *Desalination* **287** (2012) 159–166.

[19] H. Chang, C.-L. Chang, C.-Y. Hung, T.-W. Cheng, C.-D. Ho, Optimization study of small-scale solar Membrane Distillation desalination systems (s-SMDDS), *Int. J. Environ. Res. Public Health* **11** (2014), 12064-12087.

[20] L. Francis, N. Ghaffour, A. S. Alsaadi, S. P. Nunes, G. L. Amy, Performance evaluation of the DCMD desalination process under bench scale and large scale module operating conditions, *J. Membr. Sci.* **455** (2014) 103–112.

[21] W. Heinzl, S. Büttner, G. Lange, Industrialized modules for MED Desalination with polymer surfaces, *Des. and Water Treat.* **42** (2012) 177–180.

[22] D. Winter, J. Koschikowski, M. Wieghaus, Desalination using Membrane Distillation: Experimental studies on full scale spiral wound modules, *J. Membr. Sci.* **375** (2011) 104–112.

[23] E. K. Summers, H. A. Arafat, J. H. Lienhard, Energy efficiency comparison of single-stage Membrane Distillation (MD) desalination cycles in different configurations, *Desalination* **290** (2012) 54–66.

[24] S. Wardeh, H. P. Morvan, CFD simulations of flow and concentration polarization in spacer-filled channels for application to water desalination, *Chem. Eng. Res. and Des.* **86** (2008) 1107–1116.

Appendix: Nusselt number in parallel channel flow for different thermal boundary conditions

Although, in the present paper, the attention is focused on complex, spacer-filled channels (which can only be studied by means of fully three-dimensional numerical simulations), in order to appreciate the influence of thermal boundary conditions on heat transfer it is instructive to consider a simpler, essentially one-dimensional, problem (plane Poiseuille flow) since it leads to ordinary differential equations which can be solved to a very high accuracy. The mathematical treatment and the results obtained can easily be adapted also to mass transfer with obvious changes.

Consider the steady, hydrodynamically and thermally fully developed flow of a constant-property fluid in a plane channel of half-thickness δ. Let x be the streamwise direction and y the cross stream one, with y=0 at the midplane, and let $u(y)$ be the velocity along x, U its average, $T(x, y)$ the temperature and $\alpha=\lambda/(\rho c_p)$ the thermal diffusivity.

Consider first the case of symmetric two-side cooling, which can be characterized by a symmetry condition at the midplane and a general (3rd type) boundary conditions at one wall:

$$\left[\frac{\partial T}{\partial y}\right]_0 = 0; \quad -\lambda\left[\frac{\partial T}{\partial y}\right]_\delta = \frac{1}{r}[T(x,\delta) - T_\infty] \tag{A.1}$$

T_∞ being a uniform external temperature and r an interposed thermal resistance. Let $\vartheta=T-T_\infty$ and

$$\vartheta_b = \frac{1}{2\delta\rho U}\int_{-\delta}^{\delta} \vartheta\, u\, dy \tag{A.2}$$

its bulk value. The following dimensionless variables can be introduced

$$\eta \equiv \frac{y}{\delta}; \quad \xi \equiv \frac{x}{\delta}; \quad \tilde{u} \equiv \frac{u}{U}; \quad \mathrm{Pe}_\delta \equiv \frac{U\delta}{\alpha} \tag{A.3}$$

The Poiseuille velocity distribution and the energy balance equation can be written

$$\tilde{u} = \frac{3}{2}(1-\eta^2) \tag{A.4}$$

$$\frac{\partial^2\vartheta}{\partial\eta^2} = Pe_\delta\,\tilde{u}\,\frac{\partial\vartheta}{\partial\xi} \tag{A.5}$$

The assumption of thermally fully developed flow implies

$$\vartheta=\vartheta_b(x)\,\varphi(y) \tag{A.6}$$

so that Eq. (A.5) can be written

$$\frac{1}{\varphi\tilde{u}}\frac{\partial^2\varphi}{\partial\eta^2} = Pe_\delta\,\frac{\partial\vartheta_b}{\partial\xi} \tag{A.7}$$

Following the method of separation of variables, Eq. (A.7) splits into the two distinct equations

$$\frac{1}{\varphi\tilde{u}}\frac{\partial^2\varphi}{\partial\eta^2} = -B^2 \tag{A.8}$$

$$\mathrm{Pe}_\delta\,\frac{1}{\vartheta_b}\frac{\mathrm{d}\vartheta_b}{\mathrm{d}\xi} = -B^2 \tag{A.9}$$

in which the constant $-B^2$ must be negative because, for example, $\vartheta_b>0$ implies $d\vartheta_b/d\xi<0$ (cooled fluid). By substituting the velocity profile of Eq. (A.4) into Eq. (A.8) one obtains

$$\frac{\mathrm{d}^2\varphi}{\mathrm{d}\eta^2} + \frac{3}{2}B^2(1-\eta^2)\varphi = 0 \tag{A.10}$$

This is a non-integrable ODE with non-constant coefficients which can easily be solved numerically. The boundary conditions for φ are derived from eqs. (A.4) and (A.6):

$$\left[\frac{\partial \varphi}{\partial \eta}\right]_0 = 0; \quad \varphi(1) = B^2 R \tag{A.11}$$

in which $R=r\lambda/\delta$ (dimensionless thermal resistance). The following condition must also be satisfied:

$$\left[\frac{\partial \varphi}{\partial \eta}\right]_1 = -B^2 \tag{A.12}$$

which is derived from the enthalpy balance:

$$-\lambda\left[\frac{\partial \vartheta}{\partial y}\right]_\delta = -\delta \rho c_p U \frac{d\vartheta_b}{dx} \tag{A.13}$$

Conceptually, Eq. (A.10) for $\varphi(\eta)$, with B.C.'s (A.11), must be solved numerically for each generic B^2, and B^2 has to be varied so as to satisfy Eq. (A.12). A simple iterative procedure was implemented in Fortran to perform this calculation. After convergence, the heat transfer coefficient is

$$h = \frac{q''_w}{\vartheta_b} = -\frac{\lambda}{\delta \vartheta_b}\left[\frac{d\vartheta}{d\eta}\right]_\delta \tag{A.14}$$

which can be made dimensionless as a Nusselt number $\mathrm{Nu}=h(4\delta/\lambda)$ (based on the channel hydraulic diameter 4δ). From the above equations and definitions it follows that

$$\mathrm{Nu} = \frac{4}{R}\frac{\varphi(1)}{1-\varphi(1)} \tag{A.15}$$

Note that a different value of Nu and a different profile $\varphi(\eta)$ are computed for each choice of the dimensionless thermal resistance R. Note also that the Dirichlet and Neumann conditions are obtained as limiting cases for $R=0$ and $R\to\infty$, respectively. The function $\mathrm{Nu}(R)$ is represented in Figure A.1 by the "Two-side" line.

Consider now the case of one-side cooling, i.e. cooling from one wall with the opposite wall adiabatic. The thermal boundary conditions (A.1) are replaced by

$$\left[\frac{\partial T}{\partial y}\right]_{-\delta} = 0; \quad -\lambda\left[\frac{\partial T}{\partial y}\right]_\delta = \frac{1}{r}\left[T(x,\delta) - T_\infty\right] \tag{A.16}$$

and their dimensionless counterparts (A.11) are replaced by

$$\left[\frac{\partial \varphi}{\partial \eta}\right]_{-1} = 0; \quad \varphi(1) = 2B^2 R \tag{A.17}$$

while all other equations and definitions remain unchanged. The solution for Nu is reported in Figure A.1 as the "One-side" line. Note the lower levels of Nu with respect to the "Two-side" case.

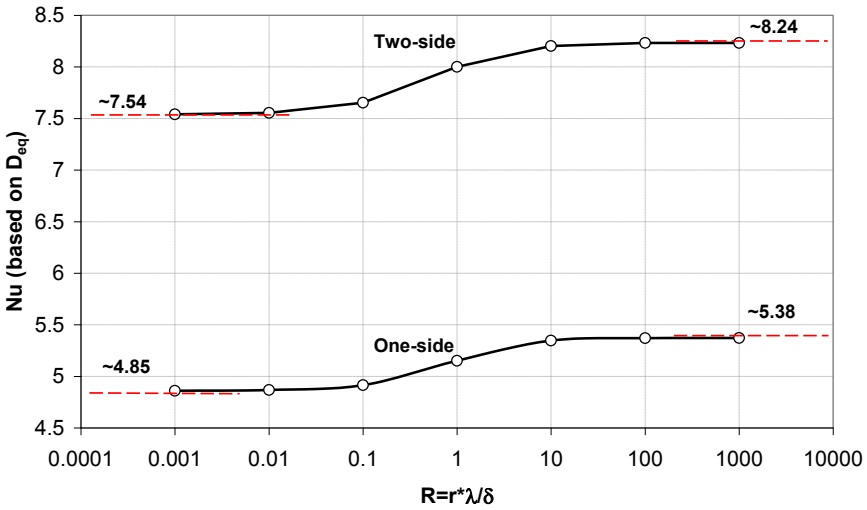

Figure A.1 Nusselt number in a plane channel as a function of the dimensionless thermal resistance *R*.